HHS Public Access

Author manuscript

Curr Biol. Author manuscript; available in PMC 2017 August 08.

Published in final edited form as:

Curr Biol. 2016 August 08; 26(15): 1935–1942. doi:10.1016/j.cub.2016.05.051.

Identification of a retinal circuit for recurrent suppression using indirect electrical imaging

Martin Greschner[1,2], **Alexander K. Heitman**[2], **Greg D. Field**[3,2], **Peter H. Li**[2], **Daniel Ahn**[2], **Alexander Sher**[4], **Alan M. Litke**[4], and **E.J. Chichilnisky**[5]

[1]Department of Neuroscience, Carl von Ossietzky University, Oldenburg 26129, Germany

[2]Systems Neurobiology, The Salk Institute for Biological Studies, La Jolla, California 92037

[3]Department of Neurobiology, Duke University School of Medicine, Durham, North Carolina 27710

[4]Santa Cruz Institute for Particle Physics, University of California, Santa Cruz, California 95064

[5]Departments of Neurosurgery and Ophthalmology, and Hansen Experimental Physics Laboratory, Stanford University, Stanford, California 94305

Summary

Understanding the function of modulatory interneuron networks is a major challenge, because such networks typically operate over long spatial scales and involve many neurons of different types. Here we use an indirect electrical imaging method to reveal the function of a spatially extended, recurrent retinal circuit composed of two cell types. This recurrent circuit produces peripheral response suppression of early visual signals in the primate magnocellular visual pathway. We identify a type of polyaxonal amacrine cell physiologically via its distinctive electrical signature, revealed by electrical coupling with ON parasol retinal ganglion cells recorded using a large-scale multi-electrode array. Coupling causes the amacrine cells to fire spikes that propagate radially over long distances, producing GABA-ergic inhibition of other ON parasol cells recorded near the amacrine cell axonal projections. We propose and test a model for the function of this amacrine cell type, in which the extra-classical receptive field of ON parasol cells is formed by reciprocal inhibition from other ON parasol cells in the periphery, via the electrically coupled amacrine cell network.

eTOC blurb

Greschner et al. discovered an amacrine subcircuit that recurrently modulates the activity of retinal ganglion cells in the magnocellular visual pathway of primates. The amacrine cells are electrically

Corresponding author: Martin Greschner, martin.greschner@uni-oldenburg.de.

Competing interests: none

Author contributions

M.G., A.K.H., G.D.F., P.H.L., D.A., A.S. and E.J.C. conducted the experiments, M.G., A.M.L., E.J.C. designed the experiments, M.G., A.K.H. and E.J.C. wrote the paper.

coupled to ON-parasol cells, and their signals propagate over long distances, producing reciprocal inhibition of distant ON-parasol cells.

Introduction

A major feature of visual processing is recurrent response normalization, which accounts for diverse aspects of modulation of light responses outside of the classical receptive field of visual neurons [1, 2]. However, understanding the specific cell types and circuits that produce such normalization is difficult, because of the challenges associated with recording many interacting cells of different types over large regions.

In the retina, response modulation outside the classical receptive field has long been observed [3–10]. Specifically, in several types of retinal ganglion cells (RGCs), activity due to excitation in the receptive field center can be modulated by stimuli far outside the receptive field. An interesting candidate for the circuit mechanism is a collection of anatomically identified polyaxonal amacrine cell (PAC) types, which have radially projecting axonal arbors that extend for millimeters over the retinal surface, resulting in long-range connectivity well-suited to serve as a mechanism for peripheral response modulation. The PACs are thought to pool rectified synaptic inputs from bipolar cells and probably provide inhibitory synaptic inputs to RGCs and bipolar cell terminals [11, 12]. Their long axonal processes probably require that these cell fire spikes to transmit their signals. Recently, we identified and characterized a spiking polyaxonal amacrine cell type in the primate retina which could play such a role [13]. However, no interaction with the 5 major primate ganglion cell types was observed. This suggests that other amacrine cell types which have not yet been recorded may play an important modulatory role in the neural pathways responsible for high-resolution vision.

Here we exploit the fact that several amacrine cell types are gap junction coupled to specific retinal ganglion cell types (e.g. [14, 15]) to target and characterize a previously unrecorded PAC in the primate retina that is electrically coupled to ON parasol ganglion cells [16, 17]. ON parasol cells are frequently sampled in extracellular recordings [18] and subserve one of the major primate retino-geniculate visual pathways [19]. Using large-scale multi-electrode recordings, and a novel analysis of electrical imaging that leverages coupling, we reveal a type of PAC on the basis of coupling to ON parasol cells. We find that these PACs exhibit electrical features broadly similar to the PACs previously studied, and closely mirror the activity of the ON parasol cells to which they are coupled. Furthermore, they transmit their spiking output signals over several millimeters of the retina, modulating responses of other ON parasol cells near their axons via GABA-ergic inhibition. This circuit architecture yields a surprising hypothesis for the function of the PACs, namely, that they provide recurrent inhibition of visual signals in ON parasol cells, rather than feed-forward inhibition from the bipolar cell network. We propose and test a quantitative model in which the extra-classical receptive field of ON parasol cells is formed by this recurrent inhibitory mechanism.

Results

Multi-electrode recordings and indirect electrical imaging of polyaxonal amacrine cells

To identify amacrine cell types interacting electrically with retinal ganglion cells (RGCs), the electrical signatures of RGCs were analyzed in large-scale multi-electrode recordings. The spikes of hundreds of RGCs of several types were sorted on the basis of their characteristic spatio-temporal waveforms [20, 21] (see Methods). ON and OFF parasol cells, two of the five numerically dominant RGC types in primate retina, were identified by their characteristic density and light responses [21, 18]. Then, using all the spike times of a given parasol cell, the average voltage waveform over all electrodes near the time of the spike was calculated [20, 22, 13] (Fig. 1B,C). This *electrical image* revealed the average spatiotemporal pattern of voltage deflections recorded over the array during and after the occurrence of spikes in the parasol cell. The averaging procedure made it possible to detect and characterize small voltage deflections produced in association with the firing of the cell, including signals far from the soma.

As expected from previous work [20, 22, 13], the large biphasic somatic spike produced by the parasol cell was surrounded by a smaller opposite-sign dendritic potential on nearby electrodes, and was followed by a triphasic axonal spike propagating across the array toward the optic disc (Fig. 1B,C). These general features were common to all RGCs in the recording.

However, on closer inspection, the electrical images of ON parasol cells revealed additional structure indicating a strong interaction with a second cell type. In addition to the main axonal spike (Fig. 1C, trace 2), smaller auxiliary spikes were detected, emanating from a region near the ON parasol cell soma, and propagating simultaneously, and more slowly, in multiple directions (Fig 1C, traces 3–7) (see supplementary movie). The electrical image of the ON parasol cell and the auxiliary spike axons could be separated in time (Fig 1D), revealing the distinctive signature of the auxiliary signal. The pattern of radial spike propagation in this signal, in some cases over 3 mm (the maximum distance observable on the multi-electrode array), is consistent with only one known cell class in the retina: spiking polyaxonal amacrine cells (PACs) [13]. These auxiliary propagating signals were present in recordings of both spontaneous and visually-driven activity.

Why would the electrical image of an ON parasol cell reveal the superimposed electrical signature of a PAC? Spike sorting artifacts were unlikely, given the discrete clusters formed by the parasol cell spike waveforms and the fact that these additional PAC spikes were observed only in ON parasol cells, and not OFF parasol cells or ON or OFF midget cells. The most likely origin of these signatures is electrical coupling to a PAC. Specifically, because the electrical image is calculated by averaging voltage waveforms recorded at the times of ON parasol cell spikes, voltage fluctuations in any cell that fires spikes in a precise temporal relationship to the ON parasol cell spikes will appear in the electrical image. Previous anatomical work has revealed a type of PAC that is tracer-coupled, and thus presumably electrically coupled, to ON parasol cells [16, 17]. Strong electrical coupling would be expected to produce spikes in these PACs in a precise temporal relationship to spikes in the ON parasol cell. Based on these considerations, the auxiliary axons in electrical

images of ON parasol cells were interpreted as revealing spikes from electrically coupled PACs.

Physiological properties of coupled polyaxonal amacrine cells

The interpretation that the auxiliary axons originate from electrically coupled PACs was supported by blockade of gap junction coupling using meclofenamic acid (20 μM) [23, 24] (Fig. 2A). This blockade reduced the magnitude of auxiliary axon signals in the electrical image relative to the strength of the primary axon signal. Since the electrical image is the average voltage waveform around the time of a somatic spike of the reference cell, this can be interpreted as reduced coupling of the PAC and the ON parasol cell causing them to fire together less frequently. Gap junctions are commonly found between various cell types in the retina and the effects of gap junction blockers are generally hard to interpret. However, in this case, the electrical image permitted separate analysis of the coupling of the ON parasol cell and the PAC, because the same basic features appeared in the electrical image, but with a different balance. Furthermore, the reduction of PAC signal strength in the electrical image would not be expected from an overall suppression of firing by the drug, but would be expected based on reduced coupling. A concentration of 100 μM meclofenamic acid led to the complete disappearance of the auxiliary axon signals, and could be interpreted as a complete uncoupling of the ON parasol cell and PAC; however, at this concentration the overall responsiveness and health of the retina decreased strongly and recovery after wash could not be achieved.

The number of ON parasol cells which displayed detected PAC axons varied across preparations. In some preparations PAC axons could be detected in the electrical images of over 90% of ON parasol cells (e.g. in 158 from 167 ON parasol cells in Fig. 4A). The largest PAC axonal spikes identified in the electrical images of ON parasol cells were up to 10% of the amplitude of ON parasol axonal spikes. These indirectly recorded PACs (detected by their electrical coupling to ON parasol cells) were observed simultaneously with directly recorded PAC types described previously [13]. Directly recorded overlapping PACs exhibited axonal arbors spatially distinct from those in the parasol-coupled PACs. Furthermore, in some preparations the receptive fields of the directly recorded PACs formed a mosaic, indicating that nearly all cells of this type in the region had been recorded, and therefore that the parasol-coupled PACs were of a different type. The indirectly recorded PACs were observed at scotopic light levels (data not shown), in addition to the photopic light levels reported herein.

Examining the distribution of voltage amplitudes at the electrodes near PAC axons yields a rough estimate of the reliability of electrical coupling. If every ON parasol spike triggered a PAC spike, the voltage distribution at an electrode should be unimodal, whereas unreliable coupling would be expected to produce a distribution composed of voltages recorded with and without PAC spikes. The observed distribution can be modeled using variance from other portions of the voltage trace (Fig. 2B). The coupling efficiencies estimated in this way varied from cell to cell (57%, +−17% SD; 61 ON parasol cells).

Furthermore, in agreement with earlier results from different types of PACs that were directly recorded [13], the spike conduction velocity of PAC axons was much slower than

that of ON parasol cell axons (0.5m/s, +−0.1 SD; 1.5m/s, +−0.2 SD; 28 cells) (Fig. 3A). As in other PAC types, spike conduction velocity declined as a function of distance from the soma, unlike in ON parasol cell axons. To analyze the conduction velocity, the timing of axon spikes was examined as a function of distance (Fig. 3B). In all cases examined, this analysis revealed a delay between the ON parasol cell spike and the PAC spike initiation, suggesting that the parasol cell spike predominantly caused the PAC spike.

Modulation of visual signals in ON Parasol retinal ganglion cells

Many types of amacrine cells, including PACs, are known to exert an inhibitory influence on retinal ganglion cells [25]. To test whether firing of this PAC type modulated the firing of simultaneously recorded RGCs, in recordings of spontaneous activity, the spike times of the PAC (inferred from the spike times of the recorded ON parasol cell) were correlated with the spikes of other RGCs. For ON parasol cells, this analysis revealed a spatially specific pattern of interaction with the PAC (Fig. 4A). On average, the ON parasol cells lying near the axons of the PAC exhibited reduced firing after the occurrence of an inferred PAC spike, while parasol cells farther from the axons did not (Fig. 4C, D), suggesting that the PAC provided inhibitory synaptic input to other ON parasol cells. This interpretation was supported by blockade with the $GABA_A$ receptor antagonist gabazine (5 μM) (Fig 4E, F). In sum, these findings are consistent with the hypothesis that PACs are electrically coupled to ON parasols near the ON parasol cell soma, and form GABA-ergic synapses with other ON parasol cells along their axons (Fig. 5A) [17].

How does response suppression by PACs modulate visual signals transmitted to the brain by the ON parasol cells? This was examined by analyzing modulation of ON parasol cell firing in the presence of a white noise visual stimulus. To tease apart the effects of the visual stimulus and PAC inhibition, a generalized linear model (GLM) was fitted to the recorded responses [26]. In the GLM, stimulus-driven responses sum with spike-driven feedback from other cells to produce spikes via a nonlinear mechanism (Fig. 5B). The spatiotemporal light sensitivity of the GLM, and the sign and time course of the spike-dependent feedback, were fitted to data. Sample fits (Fig. 5C) show that feedback associated with PAC spikes suppressed ON parasol firing in the presence of the stimulus, with a time course similar to suppression observed with no stimulus (Fig. 4B). The coupling filter of PACs to ON parasol cells lying near their axons were suppressive on average across cells, while those of non-overlapping cells were not (Fig. 5D). Thus, response suppression by PACs is likely to modulate visual signaling in ON parasol cells.

The strong electrical coupling between the identified PACs and ON parasol cells suggests a surprising potential architecture for visual signal modulation, namely, that PAC spikes predominantly convey recurrent visual signals from the surrounding ON parasol cell population, rather than providing feed-forward inhibition. If this hypothesis is correct, one would predict similar spatial tuning properties of excitation and PAC-mediated suppression in the ON parasol network. To test this possibility, the retina was stimulated with a central modulating sinusoidal grating pattern surrounded by a larger modulating background grating [3–9]. As expected, responses of ON parasol cells with receptive fields in the central region exhibited suppression by the surround stimulus. The excitatory tuning of ON parasol cells to

sinusoidal gratings was then compared to the tuning of PAC-mediated suppression. ON parasol cells stimulated with sinusoidal gratings exhibited an excitatory frequency tuning that peaked at 0.38–0.77 cpd (Fig. 6A, 3 retinas). Introduction of a surround grating suppressed firing of central ON parasol cells, with maximum response suppression occurring at frequencies similar to the peak excitatory tuning (Fig. 6B, 0.38–0.77 cpd, 3 retinas). The similarity between ON parasol excitatory frequency tuning and surround suppression is consistent with recurrent lateral inhibition mediated by PACs. To further test the recurrent inhibition hypothesis, a re-fitted GLM (see Methods) was used to predict responses to the same combinations of central and peripheral modulating gratings. By using a strong representative PAC coupling filter in the model, a rough upper bound estimate of the number of surrounding PACs a given ON parasol cell receives a suppressive signal from was obtained: 55, 52, and 16 respectively in 3 retinas. This modeling approach reproduced the frequency tuning of surround suppression (Fig. 6C), consistent with an origin of the suppressive signal in PACs electrically coupled to remote ON parasol cells, i.e. a recurrent inhibitory network architecture.

Discussion

The indirect electrical imaging method developed here revealed the recurrent modulatory function of a network of amacrine cells in the primate retina. The electrical coupling from ON parasol cells to this amacrine cell type, and the consequent suppression of firing in other ON parasol cells over a large region, implies that a component of the extra-classical receptive field surround is assembled from the recurrent responses of other ON parasol cells, rather than a distinct network of interneurons.

A variety of peripheral response suppression effects have been demonstrated in the retina [3–6, 8, 10]. One specific example is the the amacrine cell circuit that signals the motion of objects in the visual field relative to motion of the background, in salamander and rabbit retinas [7, 9]. Although the computation is similar in the circuit studied herein, the circuit architecture is different. The computational similarity is that in both cases, the visual features driving the receptive field center and the features driving surround suppression are the same. This differs fundamentally from certain cortical normalization circuits in which the tuning of the excitatory center and the suppressive surround can be very different (see [27], typically, with surround tuning being much broader. However, despite the computational similarity between the two retinal circuits, the circuit architecture is quite different: in the ON parasol network, surround suppression is produced by recurrence via electrical coupling, while in the object motion sensing circuit, the suppressive signal is created by a parallel computation via direct bipolar inputs to amacrine cells. A possible interpretation of these findings is that retinal architecture has evolved to perform similar computations using two different circuit architectures. Another possibility is that details of the timing or spatiotemporal tuning of surround suppression differ from the center tuning in the object motion sensing circuit, in a way that has not yet been fully appreciated. Certainly, in the recurrent network revealed here, surround suppression is precisely tuned to the same spatiotemporal features as the receptive field center (Fig. 6), because both signals arise from the same ON parasol cell type. However, while the PACs closely mirror the activity of the

ON parasol cells to which they are coupled, they very likely receive additional inputs from bipolar and other amacrine cell types as well (e.g. [28]).

The anatomical identity of the recorded cells is uncertain. Earlier dye coupling studies reported that ON parasol cells were coupled to two distinct amacrine cell types: (1) a smaller type with thin, sparsely branching dendrites that extend for 1–2 mm and (2) a larger axon-bearing type with axons extending at least for 2–3 mm [16, 17]. The amacrine cell type reported here is most likely the large, axon-bearing type. The observed auxiliary axons usually extended beyond the border of the recording area (max. ~3 mm). No evidence for two distinct populations of coupled amacrine cells was observed. The mean spike waveform and spike propagation speed closely resembled those of amacrine cell types described earlier [13], which have a poly-axonal structure and probably produce classical sodium spikes [29–31].

The degree of observed coupling was variable, as in many experimental studies involving gap junctions. This variation could reflect differences in the adaptive or circadian state of the retina. Earlier studies indicated that a parasol cell is dye coupled to multiple PACs [16, 17]. In the present data, the electrical images of ON parasol cells were usually dominated by one or two cells that were presumably strongly coupled (see Fig 2A, 4A). Variations of coupling strength within a preparation could reflect a range of distances between the cell bodies of ON parasol cells and the nearest PACs of the coupled population, which could influence the probability and magnitude of gap junction coupling.

It remains to be seen whether the recurrent architecture is specific to ON parasol cells or more general in the retina. In the present data, among the major cell types (ON midgets, OFF midgets, ON parasol, OFF parasol and small bistratified cells), the ON parasol cells were the only cell type that showed electrical coupling to an amacrine cell. However, an earlier report on the tracer coupling between parasol and amacrine cells made no distinction between the coupling pattern of ON and OFF parasol cells [16], leaving open the possibility of a similar network for OFF parasol cells. It is possible that existing PAC axons in the OFF layers were not picked up by with the extracellular electrode arrays used here. However, the most prominent directly-recorded PAC type in recordings performed using the same methods has an OFF light response type [13], indicating that amacrine cells with the OFF response polarity are recordable with this approach. Furthermore, previous work revealed homotypical coupling in ON parasol cells but not OFF parasol cells [32, 33].

The recurrent inhibition observed here seems unlikely to mediate visual functions that rely on precise spike timing. Every ON parasol cell was inhibited by the low-pass filtered mean activity of roughly 50 distant ON parasol cells. Over the >3 mm length of PAC axons, spike propagation time can be >6 ms (Fig. 3A), which could introduce large temporal offsets between different inhibitory PAC inputs to a given ON parasol cell. Also, every PAC spike produced inhibition lasting on roughly 15 ms. Therefore, it seems that this mechanism produces inhibition reflecting aggregate statistics of responses, and may not be appropriate for precisely timed inhibitory functions.

Recurrent normalization of responses similar to the present results is thought to be important for diverse neural computations in visual cortex [1, 2]. The present findings indicate that this important neural computation begins in the retina.

Experimental Procedures

Retinas were obtained and recorded as described previously [20, 21]. Briefly, eyes were taken from terminally anesthetized macaque monkeys (*Macaca mulatta, M. fascicularis*), used by other laboratories in the course of their experiments, in accordance with institutional guidelines for the care and use of animals. Segments of peripheral retina were isolated from the pigment epithelium, and placed flat, ganglion cell side down, on a planar array of extracellular microelectrodes. Two different electrode arrays of 512 electrodes were used. One array covered a rectangular region 1890 × 900 μm, the second a hexagonal region 3120 μm wide. While recording, the retina was perfused with Ames' solution (33–36°C) bubbled with 95% O2 and 5% CO2, pH 7.4. The light intensity was kept constant across experiments at 830 (840, 440) P* (L (M, S) cone) $^{-1}$ s^{-1}. The display was calibrated using a PR-701 spectroradiometer (Photo-Research, Chatsworth, CA, USA) and a photodiode (UDT Instruments, San Diego, CA, USA). The photopic photon absorption rates were computed assuming a 0.37 μm^2 collecting area for primate cones [34]. In addition, the indirectly recorded PACs were observed across at light levels from 4500 P* rod^{-1} s^{-1} (corresponds to 1550 (1570, 740) P* (L (M, S) cone) $^{-1}$ s^{-1}) to 0.05 P* rod^{-1} s^{-1} (data not shown).

Recordings were analyzed off-line to isolate the spikes of different cells, as described previously [21, 18]. Briefly, candidate spike events were detected using a threshold on each electrode, and the voltage waveforms on the electrode and neighboring electrodes around the time of the spike were extracted. Clusters of similar spike waveforms were identified as candidate neurons if they exhibited a refractory period. Duplicate recordings of the same cell were identified by temporal cross-correlation and removed.

A white noise stimulus, composed of a lattice of square pixels updating randomly and independently of one another over time, was used to characterize the spatial, temporal, and chromatic response properties of recorded cells [35]. The spike-triggered average stimulus obtained in response to white noise was taken as a summary of the spatio-temporal-chromatic light response properties of the cell. The receptive fields were summarized by fitting the STA with a two-dimensional elliptical Gaussian function. These receptive fields fits were visualized by an ellipse for each cell representing the 1 SD contour of the Gaussian (Fig. 1A). Correspondences between functionally defined ganglion cell types, and previously identified morphologically distinct ganglion cell types (e.g. ON parasol) were inferred based on cell densities and light response properties [18].

Electrical images were calculated as the spike-triggered average electrical signal across the array for each cell separately [20, 22, 13]. Specifically, for each electrode, the voltage waveform during the time period from 0.5 ms before to several milliseconds after each spike from the cell was identified, and the average across spikes was computed. To display the electrical image, the minimum voltage deflection at each electrode was shown using the spatial layout of the electrodes, represented by the size of disk and its gray value. Largest

amplitudes were saturated to increase visibility of PAC axons. The conduction velocity of action potentials in ON parasol cells and PAC axons (Fig. 3) was estimated by a linear fit to the distance the spike traveled along the axon per unit time.

To evaluate the effects of gap junction blocker meclofenamic acid (Sigma; Fig. 2A), changes in amplitude of the electrical image of axonal spikes between control, drug and washout conditions were measured. The electrical image is the average voltage waveform around the time of a somatic spike of the reference cell. Thus, any reduction in the synchronized firing of PAC and ON parasol cell firing due to loss of coupling would be expected to reduce the contribution of the PAC to the ON parasol electrical image. Therefore, the reduction in the magnitude of apparent PAC axons was interpreted as a reduction in coupling. Meclofenamic acid was used in a low concentration (20 μM) to enable a washout. At higher concentrations (100 μM), PAC axons were no longer detected, but the stability of the recording was negatively impacted (see [36]). In order to record a sufficient number of spikes for the subsequent analysis, the drug was administered for 30–60 minutes. During this time the overall spike rate decreased, particularly in ON cells. At high concentrations no reversal of the observed effects could be obtained with a washout of over 1 hour.

Cross-correlation functions (Fig. 4B–F) were obtained by binning spikes into 1 ms time bins and computing the correlation coefficient between the resulting spike count vectors, as a function of temporal offset. ON parasol cells were classified manually into groups that did, and did not, overlap with a PAC axon. ON parasol cells very near to the reference cell body were omitted, because they exhibited strong positive correlations from shared photoreceptor noise and electrical coupling ([33, 37]).

To estimate how response suppression by PACs modulates visual signals, a generalized linear model (GLM) was fitted to the data (Fig. 5B). The GLM consists of a bias term μ, stimulus filter k, a spike-history filter h, and a set of incoming coupling filters $\{l_i\}$. The parameters act on the stimulus x, the spike train of the fitted neuron y, and the spike trains of other RGCs that could affect that firing rate of the fitted neuron $\{y_i\}$.

$$\lambda(t)=\exp(\mu+k*x(t)+h*y(t)+\{I_i\}*\{y_i\}).$$

The convex nature of the maximum likelihood estimator for the GLM guarantees that the optimal model fit is found [26].

A GLM (μ,k,h,l) was fitted to ON parasol cells one PAC at a time in the presence of a white noise stimulus. Strong coupling filters $\{l_i\}$ were found in over thirty cells across three different retinas (Fig.5C). The significant difference between the average coupling filter of cells which and did not intersected PAC axons (Fig.5D) was verified for five PACs across two different retinas.

Center-surround gratings were presented to probe the function of the proposed inhibitory PAC circuit (Fig. 6B). Six different spatial frequencies were used in the center and eight different spatial frequencies and a uniform gray were used in the surround. Each

combination was shown for 10–12 seconds in a randomized order, and repeated two to three times. Each center suppression profile (gray line) was normalized by the center spike rate while a uniform gray was presented in the surround. The black average line is a standard uniformly weighted average of the center suppression profiles.

A GLM (μ,k,h) was fit to the white noise stimulus for all cells which were used in Figure 6B. A strong representative PAC coupling filter l_{rep} with a gain loss of 15% was used to simulate PAC inhibition. Each cell then had 2 free scaling parameters (c_1*μ, c_2*k, h, l_{rep}) to refit the GLM to the drifting grating stimulus. The parameters c_1 and c_2 were fit to minimize the square difference between the observed frequency tuning curve and the GLM simulated tuning curve. Using the refitted GLM we then simulated all of the center cell models with the same stimulus conditions and durations which were used in the experiment. Surround inhibition was modeled as a Poisson process with frequency determined by the measured firing rate of surround cells (Fig. 6A) multiplied by the simulated number of PACs assumed to converge onto the ON parasol cell.

Supplementary Material

Refer to Web version on PubMed Central for supplementary material.

Acknowledgments

This work was supported by NIH Grant EY017992 (E.J.C.), VolkswagenStiftung (M.G.), Helen Hay Whitney Foundation (G.D.F.) and NSF Postdoctoral Research Fellowship 1003198 (P.H.L.). We also thank C.K. Hulse for technical assistance; M.I. Grivich, D. Petrusca, A. Grillo, P. Grybos, P. Hottowy, and S. Kachiguine for technical development; H. Fox, M. Taffe, E. Callaway, and K. Osborn for providing access to retinas; and S. Barry for machining.

References

1. Heeger DJ. Normalization of cell responses in cat striate cortex. Vis Neurosci. 1992; 9:181–198. [PubMed: 1504027]
2. Carandini M, Heeger DJ, Movshon JA. Linearity and normalization in simple cells of the macaque primary visual cortex. J Neurosci. 1997; 17:8621–8644. [PubMed: 9334433]
3. McIlwain JT. Receptive fields of optic tract axons and lateral geniculate cells: peripheral extent and barbiturate sensitivity. J Neurophysiol. 1964; 27:1154–1173. [PubMed: 14223976]
4. Levick WR, Oyster CW, Davis DL. Evidence that McIlwain's periphery effect is not a stray light artifact. J Neurophysiol. 1965; 28:555–559. [PubMed: 14328453]
5. Werblin FS. Lateral interactions at inner plexiform layer of vertebrate retina: antagonistic responses to change. Science. 1972; 175:1008–1010. [PubMed: 5009392]
6. Passaglia CL, Enroth-Cugell C, Troy JB. Effects of remote stimulation on the mean firing rate of cat retinal ganglion cells. J Neurosci. 2001; 21:5794–5803. [PubMed: 11466451]
7. Olveczky BP, Baccus SA, Meister M. Segregation of object and back-ground motion in the retina. Nature. 2003; 423:401–408. [PubMed: 12754524]
8. Zaghloul KA, Manookin MB, Borghuis BG, Boahen K, Demb JB. Functional circuitry for peripheral suppression in Mammalian Y-type retinal ganglion cells. J Neurophysiol. 2007; 97:4327–4340. [PubMed: 17460102]
9. Baccus SA, Olveczky BP, Manu M, Meister M. A retinal circuit that computes object motion. J Neurosci. 2008; 28(27):6807–6817. [PubMed: 18596156]
10. Hoggarth A, McLaughlin AJ, Ronellenfitch K, Trenholm S, Vasandani R, Sethuramanujam S, Schwab D, Briggman KL, Awatramani GB. Specific wiring of distinct amacrine cells in the

directionally selective retinal circuit permits independent coding of direction and size. Neuron. 2015 Apr 8; 86(1):276–91. [PubMed: 25801705]

11. Demb JB, Haarsma L, Freed MA, Sterling P. Functional circuitry of the retinal ganglion cell's nonlinear receptive field. J Neurosci. 1999; 19(22):9756–67. [PubMed: 10559385]
12. Demb JB, Zaghloul K, Haarsma L, Sterling P. Bipolar cells contribute to nonlinear spatial summation in the brisk-transient Y-ganglion cell in mammalian retina. J Neurosci. 2001; 21:7447–7454. [PubMed: 11567034]
13. Greschner M, Field GD, Li PH, Schiff ML, Gauthier JL, Ahn D, Sher A, Litke AM, Chichilnisky EJ. A polyaxonal amacrine cell population in the primate retina. J Neurosci. 2014; 34(10):3597–3606. [PubMed: 24599459]
14. Marc RE, Jones BW. Molecular Phenotyping of Retinal Ganglion Cells. Journal of Neuroscience. 2002; 22(2):413–427. [PubMed: 11784786]
15. Völgyi B, Chheda S, Bloomfield SA. Tracer coupling patterns of the ganglion cell subtypes in the mouse retina. J Comp Neurol. 2009; 512(5):664–687. [PubMed: 19051243]
16. Dacey DM, Brace S. A coupled network for parasol but not midget ganglion cells in the primate retina. Vis Neurosci. 1992; 9(3–4):279–290. [PubMed: 1390387]
17. Jacoby R, Stafford D, Kouyama N, Marshak D. Synaptic inputs to ON parasol ganglion cells in the primate retina. J Neurosci. 1996; 16(24):8041–8056. [PubMed: 8987830]
18. Field GD, Sher A, Gauthier JL, Greschner M, Shlens J, Litke AM, Chichilnisky EJ. Spatial properties and functional organization of small bistratified ganglion cells in primate retina. J Neurosci. 2007; 27(48):13261–13272. [PubMed: 18045920]
19. Perry VH, Oehler R, Cowey A. Retinal ganglion cells that project to the dorsal lateral geniculate nucleus in the macaque monkey. Neuroscience. 1984; 12(4):1101–1123. [PubMed: 6483193]
20. Litke AM, Bezayiff N, Chichilnisky EJ, Cunningham W, Dabrowski W, Grillo AA, Grivich M, Grybos P, Hottowy P, Kachiguine S. What does the eye tell the brain? Development of a system for the large-scale recording of retinal output activity. IEEE Trans Nucl Sci. 2004; 51:1434–1440.
21. Frechette ES, Sher A, Grivich MI, Petrusca D, Litke AM, Chichilnisky EJ. Fidelity of the ensemble code for visual motion in primate retina. J Neurophysiol. 2005; 94(1):119–135. [PubMed: 15625091]
22. Petrusca D, Grivich MI, Sher A, Field GD, Gauthier JL, Greschner M, Shlens J, Chichilnisky EJ, Litke AM. Identification and characterization of a Y-like primate retinal ganglion cell type. J Neurosci. 2007; 27:11019–11027. [PubMed: 17928443]
23. Pan F, Mills SL, Massey SC. Screening of gap junction antagonists on dye coupling in the rabbit retina. Vis Neurosci. 2007; 24(4):609–18. [PubMed: 17711600]
24. Veruki ML, Hartveit E. Meclofenamic acid blocks electrical synapses of retinal AII amacrine and on-cone bipolar cells. J Neurophysiol. 2009; 101(5):2339–47. [PubMed: 19279153]
25. Masland RH. The neuronal organization of the retina. Neuron. 2012; 76(2):266–280. [PubMed: 23083731]
26. Pillow JW1, Shlens J, Paninski L, Sher A, Litke AM, Chichilnisky EJ, Simoncelli EP. Spatio-temporal correlations and visual signaling in a complete neuronal population. Nature. 2008; 454(7207):995–999. [PubMed: 18650810]
27. Carandini M, Heeger DJ. Normalization as a canonical neural computation. Nat Rev Neurosci. 2011; 13(1):51–62. [PubMed: 22108672]
28. Murphy-Baum BL, Taylor WR. The Synaptic and Morphological Basis of Orientation Selectivity in a Polyaxonal Amacrine Cell of the Rabbit Retina. J Neurosci. 2015; 35(39):13336–50. [PubMed: 26424882]
29. Stafford DK, Dacey DM. Physiology of the A1 amacrine: a spiking, axon-bearing interneuron of the macaque monkey retina. Vis Neurosci. 1997; 14(3):507–22. [PubMed: 9194317]
30. Davenport CM, Detwiler PB, Dacey DM. Functional polarity of dendrites and axons of primate A1 amacrine cells. Vis Neurosci. 2007; 24(4):449–57. [PubMed: 17550636]
31. Manookin MB, Puller C, Rieke F, Neitz J, Neitz M. Distinctive receptive field and physiological properties of a wide-field amacrine cell in the macaque monkey retina. J Neurophysiol. 2015; 114(3):1606–16. [PubMed: 26133804]

32. Shlens J, Rieke F, Chichilnisky E. Synchronized firing in the retina. Curr Opin Neurobiol. 2008; 18(4):396–402. [PubMed: 18832034]

33. Trong PK, Rieke F. Origin of correlated activity between parasol retinal ganglion cells. Nat Neurosci. 2008; 11(11):1343–1351. [PubMed: 18820692]

34. Schnapf JL, Nunn BJ, Meister M, Baylor DA. Visual transduction in cones of the monkey Macaca fascicularis. J Physiol. 1990; 427:681–713. [PubMed: 2100987]

35. Chichilnisky EJ. A simple white noise analysis of neuronal light responses. Network. 2001; 12:199–213. [PubMed: 11405422]

36. Kuo SP, Schwartz GW, Rieke F. Nonlinear Spatiotemporal Integration by Electrical and Chemical Synapses in the Retina. Neuron. 2016; 90(2):320–32. [PubMed: 27068789]

37. Greschner M, Shlens J, Bakolitsa C, Field GD, Gauthier JL, Jepson LH, Sher A, Litke AM, Chichilnisky EJ. Correlated firing among major ganglion cell types in primate retina. J Physiol. 2011; 589:75–86. [PubMed: 20921200]

Highlights

- Polyaxonal amacrine cell (PAC) type is electrically coupled to ON parasol cells
- PAC responses closely mirror those of coupled ON parasol cells
- PAC spikes propagate outward, producing GABA-ergic inhibition of ON parasol cells
- PAC network produces reciprocal peripheral suppression in ON parasol population

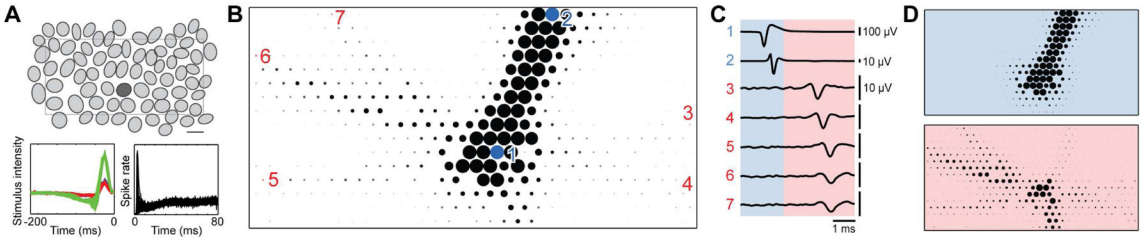

Figure 1.

The electrical image of ON parasol cells reveals unexpected radially propagating axons. **A.** Mosaic of simultaneously recorded ON parasol cell receptive fields (top) (scale bar 200 µm), overlaid spike-triggered average response time course (lower left) and autocorrelation of firing (lower right). **B.** Electrical image of a single ON parasol cell (marked dark gray in A), on the multi-electrode array (32×16 electrodes, 60 µm spacing). Size of disk and gray value represent minimal voltage deflection on each electrode. Largest amplitudes are saturated to increase visibility of PAC axons. **C.** Average voltage traces of electrodes marked in B during a recorded spike in the ON parasol cells, with characteristic somatic (trace 1) and axonal waveforms of ON parasol cell (trace 2) and PAC (trace 3–7). Blue and red regions indicate times before and after a time point 0.85 ms after the largest negative voltage deflection at the soma. **D.** Electrical image before (blue) and after (red) a time point 0.85 ms after minimal voltage deflection, revealing distinct spatial patterns.

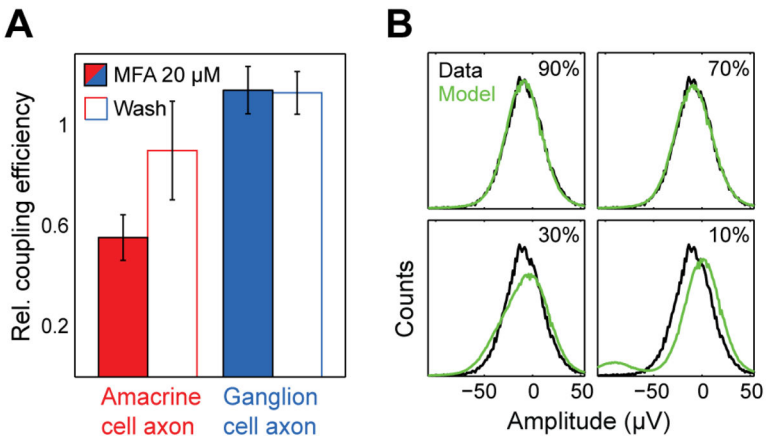

Figure 2.

Electrical coupling between ON parasol retinal ganglion cells and polyaxonal amacrine cells (PACs) produces the radial axonal electrical images. **A.** Relative estimated coupling strength between ON parasol cells and PACs (i.e. relative signal amplitude in the electrical image) in the presence and absence of gap junction blocker meclofenamic acid (MFA, 20 µM). Error bars indicate SD over 7 cells. Values are shown relative to the control condition. **B.** Unimodal distribution of voltage values indicates high coupling efficiency between PACs and ON parasol cells. Distribution of peak voltage deflection values on a single electrode along the PAC axon are shown in black. Model prediction for various spiking probabilities while maintaining identical mean amplitude. Best-fitted estimate of observed distribution in H is given by a coupling coefficient (probability of PAC spike given the occurrence of an ON parasol spike) of 86%.

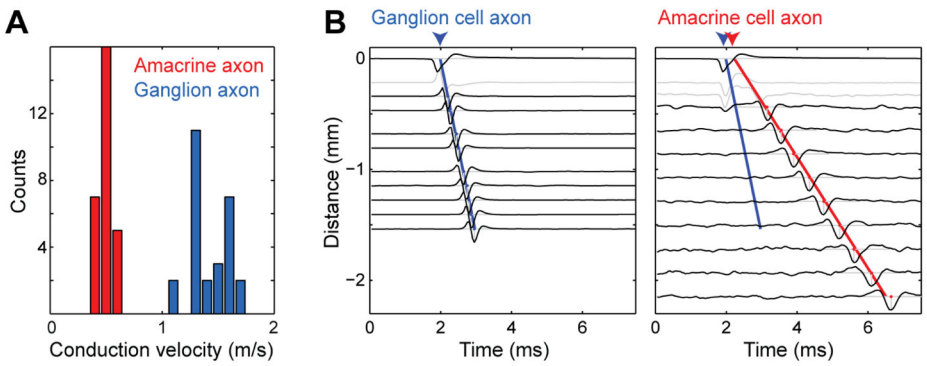

Figure 3.

Spike conduction velocity of PAC axons was much slower than that of the ON parasol axon. **A.** Distribution of conduction velocities of ON parasol cell axons and PAC axons in a single recording (28 cells). Mean:1.5m/s +−0.2 SD, 0.5m/s +−0.1 SD respectively. **B.** Voltage waveforms from electrodes obtained at different distances from the soma along the ON parasol cell and PAC axon. Time of spike initiation at the soma was linearly extrapolated toward zero from axon spike times (ON parasol axon blue line, PAC axon red), resulting in an estimated delay between ON parasol and PAC spike initiation. Dendritic waveforms were not used and are indicated in light gray. Waveform amplitudes are normalized.

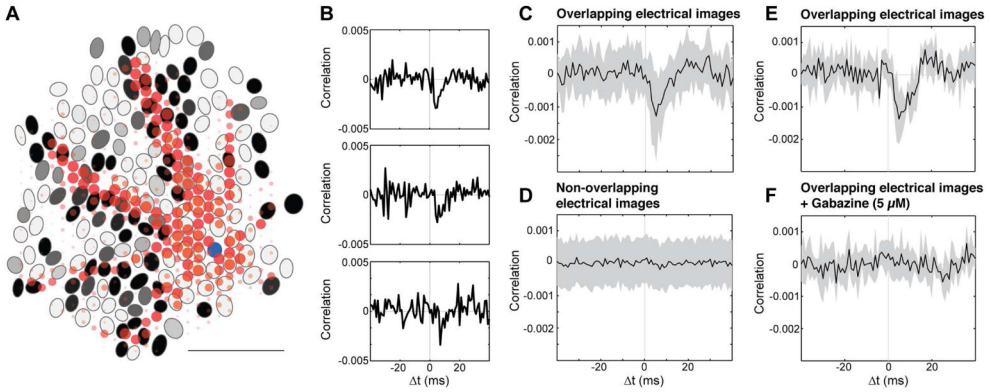

Figure 4.

Spontaneous activity of ON parasol cells near PAC axons is suppressed by PAC firing. **A.** Electrical image of one PAC (red) coupled to one ON parasol cell (receptive field in blue), aligned with receptive field mosaic of all simultaneously recorded ON parasol cells. Grayscale for ON parasol cells indicates amplitude of negative correlations of spontaneous activity between that cell and the original ON parasol cell (minimum observed correlation coefficient=−0.0042). Correlations were measured in an 8 ms time interval, shifted according to the conduction time along PAC axon. Electrical image is shown for 2–6 ms after the ON parasol somatic spike, as in Fig 1D lower panel. Scale bar 1 mm. **B.** Cross-correlation function for ON parasol cells overlapping with one PAC axon, revealing deflections suggestive of response suppression. Distance between putative PAC soma and ON parasol cells increases from the top to the bottom panels. Bin size 1 ms. **C, D.** ON parasol cells with somas near and far from the axons of the PAC were suppressed and not, respectively. Near and far ON parasol cells were separated based on their electrical image overlap with the electrical image of the PAC. Traces show cross-correlation functions, averaged across cells after adjustment for conduction time along the PAC axon. Neighboring ON parasol cells exhibited strong positive correlations due to shared input and direct coupling (see Methods), and thus were excluded from analysis. Bin size 1 ms, shaded area ±1SD, 18 overlapping, 118 non overlapping cells. **E.** As C, different preparation. Shaded area ±1SD, 10 ON parasol cells and one PAC. **F.** Negative correlations blocked by 5 μM gabazine (SR-95531). As E. Separate preparations were used for A, B-D and E–F.

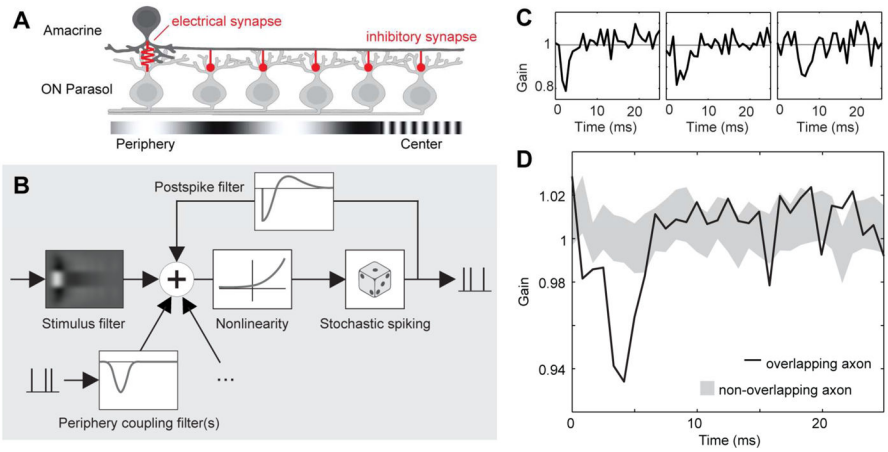

Figure 5.

The PAC network recurrently inhibits light responses of ON parasol cells. **A.** Schematic model of hypothesized PAC-mediated lateral inhibitory network. **B.** Schematic of the generalized linear model (GLM) used to summarize and analyze light responses and lateral inhibition of ON parasol cells. The spike rate controlling the model output is a nonlinear function of the sum of the filtered stimulus, filtered spike trains representing inputs from PACs, and a post-spike feedback filter internal to the cell. **C.** Individual fitted coupling filters representing PAC inputs, which modulate the gain of light driven inputs to the modeled ON parasol cell. All filters were fitted to data obtained in the presence of a white noise stimulus. **D.** Average coupling filter associated with 20 ON parasol cells overlying PAC axon (dark line) and mean±SD of filters associated with 20 ON parasol cells (resampled from ~150 cells) not overlying PAC axon (gray range). Filters adjusted for conduction time along the PAC axon prior averaging. Same preparation as Fig. 4B–D

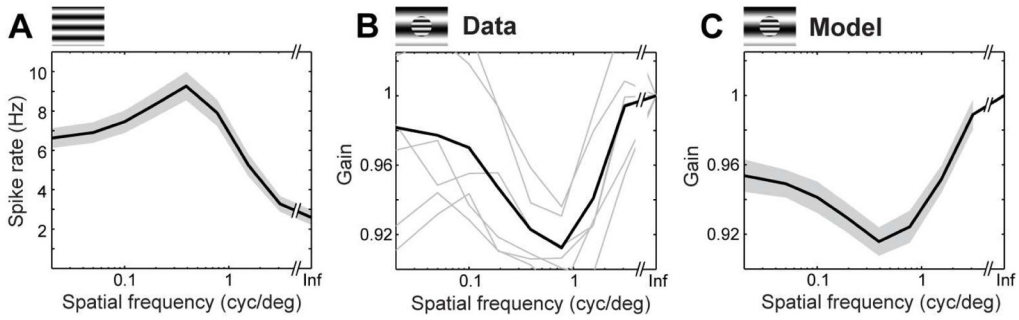

Figure 6.

Model of recurrent inhibition reproduces extra classical receptive field effects in ON parasol cells. **A.** Spatial frequency tuning of ON parasol cells to full-field sinusoidal drifting gratings (at 4 Hz; n=89), shaded region ± 1 SD. **B.** Normalized response to central grating pattern, as a function of spatial frequency of a surrounding grating pattern (10 degree center diameter). Each gray line represents a specific central grating frequency (0.77, 0.38, 0.19, 0.1, 0.05, 0.02 cyc/deg; at 4 Hz); black line represents average (n=13 ON parasol cells). **C.** Refitted GLM simulations of surround suppression using fits of the model to data from the same cells as in panel F (see Methods). Insets on top A–C indicate stimulus.